ISSN 0023-1584, Kinetics and Catalysis, 2008, Vol. 49, No. 2, pp. 271–278. © MAIK "Nauka/Interperiodica" (Russia), 2008.
Original Russian Text © A.A. Shutilov, G.A. Zenkovets, G.N. Kryukova, V.Yu. Gavrilov, E.A. Paukshtis, A.I. Boronin, S.V. Koshcheev, S.V. Tsybulya, 2008, published in Kinetika i Kataliz, 2008, Vol. 49, No. 2, pp. 284–292.

Effect of the Microstructure of Pt/CeO_2–TiO_2 Catalysts on Their Catalytic Properties in CO Oxidation

A. A. Shutilov, G. A. Zenkovets, G. N. Kryukova, V. Yu. Gavrilov, E. A. Paukshtis, A. I. Boronin, S. V. Koshcheev, and S. V. Tsybulya

Boreskov Institute of Catalysis, Siberian Branch, Russian Academy of Sciences, Novosibirsk, 630090 Russia
e-mail: zenk@catalysis.ru

Received December 11, 2006

Abstract—The microstructure of 2% Pt/CeO_2–TiO_2 catalysts has an effect on their catalytic properties in CO oxidation. The nanostructured catalysts as platinum clusters 0.3–0.5 nm in size are the most active. These clusters are stabilized at crystal boundaries formed by irregularly intergrown anatase particles. The catalyst containing platinum particles 2–5 nm in size is less active because of the decrease in the extent of dispersion of platinum and the change of its electron state.

DOI: 10.1134/S0023158408020158

Noble metals supported on Al_2O_3, TiO_2, and ZrO_2 are the most active catalysts for CO oxidation into CO_2 [1–3], which is among the most important processes of environmental catalysis. It is known that supported Pt/TiO_2 catalysts are very active in the photocatalytic oxidation of organic pollutions, such as acetaldehyde, 1-butanol, ethanol, trichloroethylene, and benzene, in air and water [3–7].

The study of physicochemical and catalytic properties of supported platinum catalysts demonstrated the strong dependence of their activity on the structure and size of platinum particles, on their distribution on the support surface, and on their interaction with the support [8–13]. The morphology and electronic properties of metal particles whose size is between a few nanometers and several tens of nanometers are of greatest interest. As the particle size decreases, the fraction of the surface atoms of supported metal increases. This is true also for the fraction of edges and corners, which can be considered as structure defects [9–13]. As is shown in [14], the electronic structure of supported metal nanoparticles also may depend on their size. The largest particle size at which one can expect changes in electronic properties was estimated at ~2 nm.

The first attempts to establish a correlation between the activity of supported metal catalysts and the metal particle size were made by Kobozev [15]. Later, it was shown that catalytic activity in many cases depends on the extent of dispersion of supported metal [16–23]. However, not in all cases does it increase with decreasing metal particle size [24–27]. For instance, the activity of 2% Pt/SiO_2 and 2% Pt/γ-Al_2O_3 catalysts in CO oxidation increases as the platinum particle size increases from 1.8 to 5.0 nm [26, 27].

The study of the microstructure effects on the catalytic properties of supported platinum catalysts in CO oxidation is essential for gaining a deeper insight into this problem and for development of new efficient catalysts. Here, we report a detailed investigation of the effect of the microstructure of Pt/CeO_2–TiO_2 samples on their catalytic properties in CO oxidation.

EXPERIMENTAL

Pt/CeO_2–TiO_2 catalysts (2 wt % Pt + 5 wt % CeO_2 + 93 wt % TiO_2) with various microstructures were prepared according to the following procedure. The support (titanium dioxide modified with cerium dioxide) was synthesized by the impregnation of anatase with a cerium nitrate solution followed by drying and thermal treatment at 500°C. For the preparation of a sample containing ultrafine platinum clusters 0.3–0.5 nm in size, the support obtained was impregnated with an appropriate amount of a platinum nitrate solution. The resulting material was dried in air at room temperature, then at 110°C for 12 h, and was calcined in air at 500°C for 4 h. For the preparation of a sample containing platinum particles 2–5 nm in size, the catalyst calcined in air was additionally calcined in flowing hydrogen (flow rate of 80 l/h) at 250°C for 2 h.

The determination of Pt, Ce, and Ti contents of the catalysts was performed by atomic-emission spectrometry with inductively coupled plasma using an Optima 4300 DV spectrometer (Perkin Elmer). The samples were dissolved in a mixture of concentrated hydrochloric and nitric acids (3 : 1) according to a published procedure [28]. The catalysts obtained were studied by X-ray diffraction, transmission electron microscopy (TEM), X-ray photoelectron spectroscopy, and adsorption methods. X-ray diffraction patterns were obtained on a URD–63 diffractometer using a graphite monochromator and CuK_α radiation. The coherent-scattering

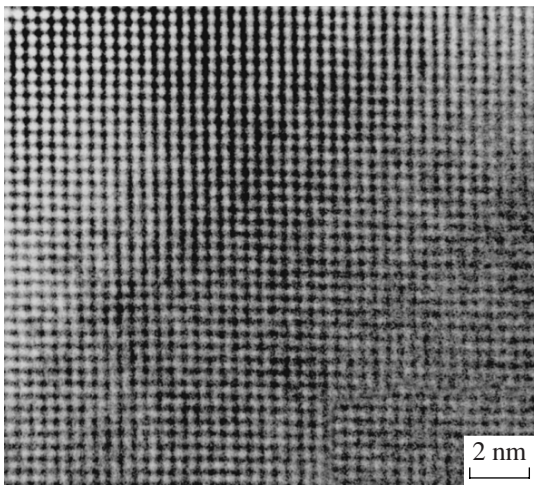

Fig. 1. Electron micrograph of the crystal structure of TiO_2 (anatase) calcined at 500°C.

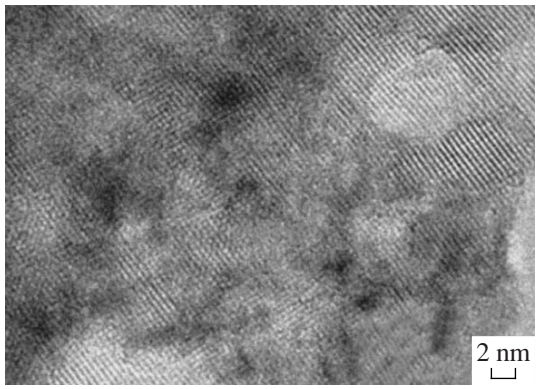

Fig. 2. Electron micrograph of the 5 wt % CeO_2 + 95 wt % TiO_2 support calcined at 500°C.

domain size for anatase crystallites (D_{CSD}) was derived from the half-width of the (200) reflection using the Scherrer equation (200) [29]. Electron microscopic examinations were carried out using a JEM-2010 instrument with 0.14 nm resolution and an accelerating voltage of 200 kV. The total surface area S (m^2/g) was measured by the thermal Ar desorption method using four sorption equilibrium points (SORBI-M instrument). The pore volume distribution over throat size was calculated from the desorption branch of the nitrogen adsorption isotherm using the Barret–Joyner–Hallenda method [30]. The measurements of low-temperature (77 K) N_2 sorption isotherms were conducted using a Digisorb-2600 Micromeritics static instrument.

The chemical composition of the catalytic surface and the oxidation states of elements were studied by X-ray photoelectron spectroscopy (XPS). Spectra were registered on an ES–300 photoelectron spectrometer (Kratos Analytical) in the constant photoelectron pass energy mode using AlK_α and MgK_α primary radiation. The energy scale of the spectrometer was calibrated against the Au $4f_{7/2}$ and Cu $2p_{3/2}$ binding energies (84.0 and 932.7 eV). When calibrating the spectra, all photoelectron lines were shifted by the value corresponding to the electrostatic shift of the Ti $2p_{3/2}$ peak (its true position for TiO_2 was taken to be 458.8 eV). Quantitative analysis was carried out using the total peak intensities of elements taking into account the atomic sensitivity factors [31, 32]. Data published in [33] were used in the processing of spectral data.

For recording the IR spectra of CO adsorbed on Pt/CeO_2–TiO_2 catalysts, the samples were pressed into pellets (~1 cm^2, 15 mg). The pellets, fixed in a special-purpose aluminum foil chuck to prevent the working beam from passing by, were placed into a spectroscopic cell. After pumping at 400°C for 2 h and cooling to room temperature, the spectrum of the initial sample was recorded. CO adsorption was conducted at room temperature and a pressure of 2.6 kPa. The IR spectra of the initial catalysts and the catalysts with adsorbed CO were recorded on a Shimadzu FTIR-8300 spectrophotometer in the range of 1000–6000 cm^{-1} with a resolution of 4 cm^{-1} for 50 signals accumulated.

Catalytic properties were studied in CO oxidation in a flow reactor. The composition of the reaction mixture was as follows: 0.05% CO, 5.0% H_2O, 6.7% air, and nitrogen as balance. Water vapor was added to the reaction mixture starting at 40°C. The GHSV of the mixture was 1.8×10^5 h^{-1}. The reaction temperature was raised at a rate of 10 K/min. The initial and resulting reaction mixtures were analyzed chromatographically. Catalytic activity was characterized by the temperature of 50% CO conversion, which was determined from the conversion versus temperature curve.

RESULTS AND DISCUSSION

We reported in [34] that the initial titanium dioxide contains fine particles 3–6 nm in size loosely packed into large aggregates ~100 nm in size. Upon calcination at 500°C, titanium dioxide transforms into anatase crystallites ~90–100 nm in size with a regular crystal structure (Fig. 1). As follows from electron microscopy data, titanium dioxide modified with cerium oxide has a markedly different structure: it appears as a nanostructured oxide (Fig. 2). This nanooxide consists of irregularly intergrown primary anatase particles forming well-defined interblock (intercrystal) boundaries. No other amorphous or crystalline phases were observed. Microanalysis data indicated the presence of cerium in these samples.

According to X-ray diffraction data, titanium dioxide modified with cerium oxide consists of anatase having standard unit cell parameters. No other crystalline phases were observed. Note that the CeO_2 phase resulting from the thermal decomposition of cerium nitrate is detected already at 350°C. Therefore, no solid solution of cerium ions in the anatase lattice forms in this case. Indeed, the crystal lattices of anatase and cerium diox-

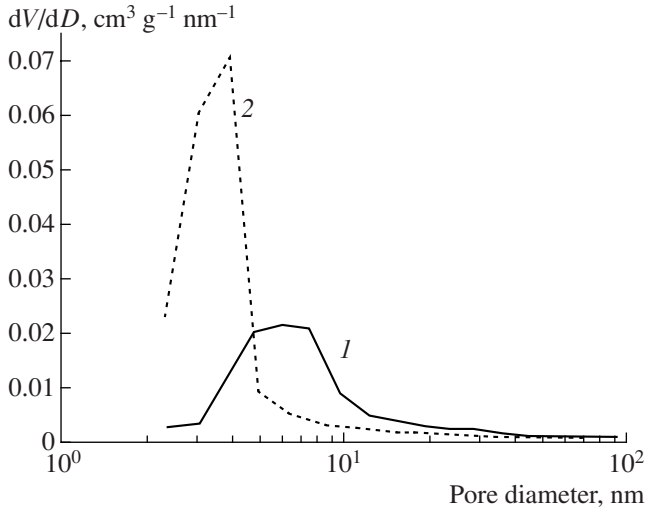

Fig. 3. Differential pore volume distribution over throat size for (*1*) TiO_2 and (*2*) 5 wt % CeO_2 + 95 wt % TiO_2 calcined at 500°C.

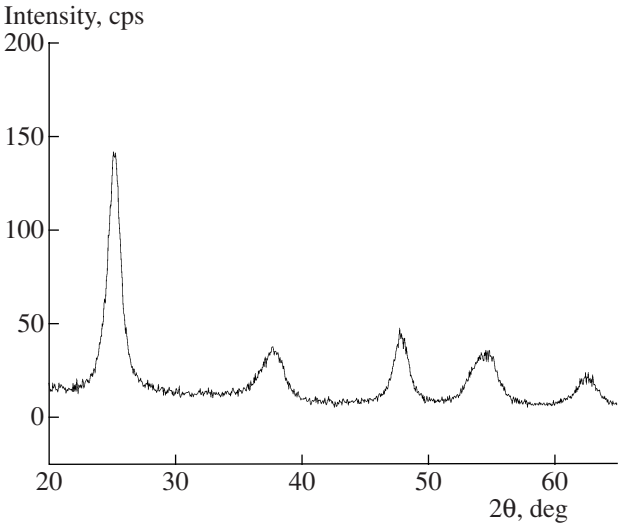

Fig. 4. X-ray diffraction pattern from the $Pt/CeO_2–TiO_2$ catalyst calcined at 500°C and containing fine (0.3–0.5 nm) platinum clusters.

ide differ essentially in parameters and structure; the ionic radii of Ti^{4+} (0.64 Å), Ce^{4+} (0.88 Å), and Ce^{3+} (1.02 Å) are also very different [35]. These facts testify against the formation of a solid solution of cerium ions in the crystal lattice of anatase. This is confirmed by the data indicating that, during heat treatment in an oxidizing medium, the formation of a titanium–cerium compound by the reaction between cerium oxide and titanium dioxide takes place only at 1300°C [36–38].

The modification of titanium dioxide with cerium oxide causes significant changes not only in the microstructure, but also in the texture. The specific surface area of pure titanium dioxide calcined at 500°C is equal to 80 m^2/g. This sample is characterized by a broad volumetric pore size distribution with a peak at 5–7 nm (Fig. 3). Titanium dioxide modified with cerium oxide is more disperse (surface area of ~200 m^2/g) and is characterized by a more homogeneous and fine-pore structure (the dominant pore size is 4 nm).

Based on the above data, we may suppose that, in these samples, cerium ions are stabilized mainly at interblock boundaries resulting from the intergrowth of primary crystallites of anatase. Apparently, this stabilization is possible due to the irregularity of the anatase crystal lattice in the intergrowth areas. The resulting cerium-modified titanium dioxide agglomerates are more disperse than the particles of unmodified TiO_2. Thus, the modified support possesses a larger specific surface area and a finer pore texture.

According to X-ray diffraction data, only the anatase phase is detectable in the $Pt/CeO_2–TiO_2$ catalyst calcined at 500°C (Fig. 4). Our electron microscopic data indicate the presence of fine platinum particles ~0.3–0.5 nm in size stabilized mainly at interblock boundaries and partly in the structure defects of anatase (Fig. 5). Simple evaluations show that the number of platinum atoms in particles of this size is as small as 3 to 6. The resulting fine clusters are sufficiently stable under the thermal treatment of the catalysts in an oxidative atmosphere. According to electron microscopy data, the morphology of the catalyst remains unchanged as the catalyst is heated in air at 350–600°C. Note that, in a previous study [39], along with the formation of platinum particles 2–3 nm in size, the formation of ultrafine platinum clusters 0.5–0.6 nm in size was observed in Pt/CeO_2 catalysts by electron microscopy. The causes of their formation were not discussed. At the same time, as was shown previously in [40], the stabilization of ultrafine platinum clusters on the anatase surface does not occur in Pt/TiO_2 catalysts. Platinum particles 3–5 nm in size were observed by electron microscopy. Apparently, it is the formation of a nanostructured support and the presence of cerium that favor

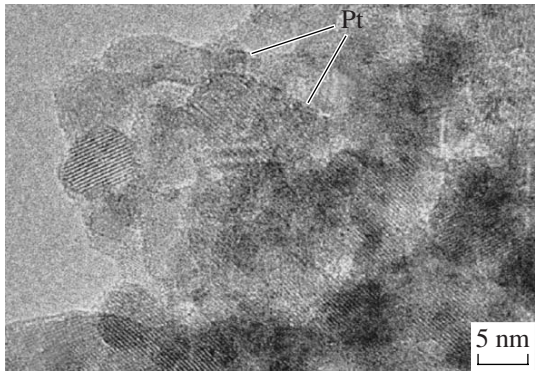

Fig. 5. Electron micrograph of the $Pt/CeO_2–TiO_2$ catalyst calcined at 500°C and containing fine (0.3–0.5 nm) platinum clusters.

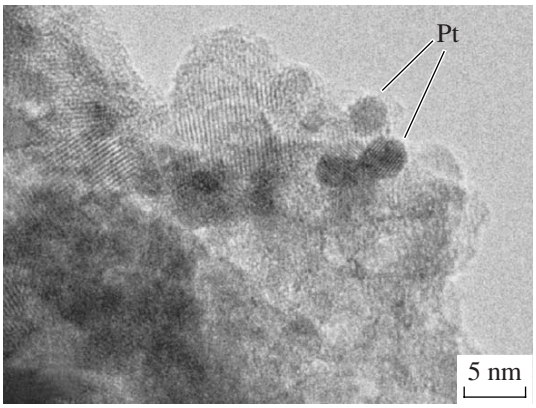

Fig. 6. Electron micrograph of the $Pt/CeO_2–TiO_2$ catalyst reduced in H_2 at 250°C, and containing platinum particles (2–5 nm).

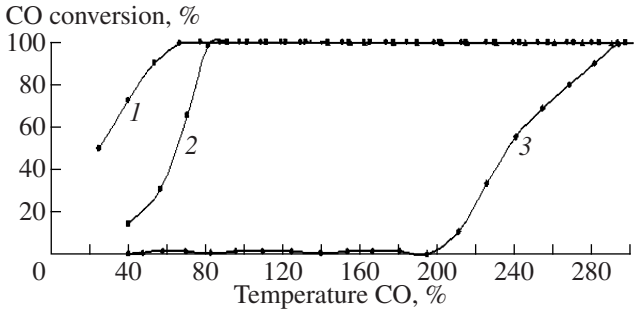

Fig. 7. The effect of temperature on CO conversion in oxidation process over $Pt/CeO_2–TiO_2$ catalysts containing (*1*) ultrafine platinum clusters (0.3–0.5 nm), and (*2*) platinum particles (2–5 nm), and (*3*) over the pure support (5% CeO_2–95% TiO_2).

the stabilization of ultrafine platinum clusters 0.3–0.5 nm in size.

Microstructural changes in the $Pt/CeO_2–TiO_2$ catalyst were induced by reducing the catalyst in flowing hydrogen at 250°C. The microstructural changes occurring during this treatment are primarily manifested as the aggregation of ultrafine platinum clusters into larger particles 2–5 nm in size. The electron micrograph presented in Fig. 6 shows such particles stabilized on the support surface. For the reductive conditions mentioned above, no changes in the structure of the support were detected by electron microscopy or X-ray diffraction.

From Fig. 7 it can be seen that $Pt/CeO_2–TiO_2$ samples with different microstructures show very different catalytic properties in CO oxidation. The $CeO_2–TiO_2$ support alone is not highly active in the oxidation of CO. The oxidation process begins only at a temperature of >190°C. The $Pt/CeO_2–TiO_2$ catalyst containing platinum clusters (0.3–0.5 nm) is the most active. The carbon monoxide conversion of 50% is attained already at 25°C, and the catalyst operates for a long time without loss of activity. The activity of the $Pt/CeO_2–TiO_2$ catalyst containing platinum particles 2–5 nm in size is slightly lower, but is still high. With this catalyst, the same conversion of 50% is attained at 68°C. Note that, according to electron microscopy and X-ray diffraction data, the structure of the catalyst remains unchanged during tests in the reaction mixture.

For the explanation of the differences between the catalytic properties of $Pt/CeO_2–TiO_2$ samples with different microstructures, we carried out an X-ray photoelectron spectroscopic study. XPS spectra recorded in the Ti $2p_{3/2}$ and O 1*s* characteristic regions are shown in Fig. 8. For both catalysts, the Ti $2p_{3/2}$ spectrum corresponds to Ti^{4+} ions in TiO_2 and indicates their homogeneity [31]. The O 1*s* spectrum shows a dominant band at ~530 eV due to O^{2-} in the TiO_2 lattice [31] and a high-energy shoulder at ~532 eV. The exact assignment of the second component is difficult to make. This component is possibly due to oxygen in the mixed oxide layer containing cerium ions along with oxygen and titanium ions. This band is also assignable to hydroxyl groups.

The Ce 3*d* lines in the spectra of both catalysts (Fig. 9) unambiguously indicate the absence of Ce^{4+} cations in the samples: the spectrum shows only 3*d* components of the spin–orbital doublet specific to the Ce^{3+} cation [41, 42]. The doublet arising from the Ce^{4+} state (its position is indicated in Fig. 9) is absent. Also absent are the two satellite lines characteristic of Ce^{4+}. Therefore, the cerium ions are only in the Ce^{3+} state.

The XPS spectra of platinum particles are shown in Fig. 10. Here we can see that the Pt 4*f* spectra of the catalysts examined are different. The positions of the Pt 4*f* component formally differ by a binding energy of ~0.6 eV. On the other hand, the curve shape shown in Fig. 10 points to a complex structure containing additional unresolved peaks. These peaks can be resolved by deconvolution after background zeroing at the left and right edges.

Figure 11 shows the doublet structure of the spectrum with the spin–orbital splitting parameters and intensities of the components actually observed in experiments [31, 32]. The spectrum deconvolution reveals the difference between the electronic states of platinum particles in the catalysts with different microstructures. Nevertheless, for particles of both types, we observe three main states with $E_b(Pt\ 4f_{7/2})$ = 70.7–70.9 eV (state I), 71.7–72.0 eV (state II), and 73.0–73.6 eV (state III). The first doublet might be assigned to Pt^0. The state of platinum with $E_b(Pt\ 4f_{7/2})$ = 73.0–73.6 eV is ionic and is close to Pt^{2+} [31–33]. The platinum state with $E_b(Pt\ 4f_{7/2})$ = 71.7–72.0 eV is also ionic and lies between the metallic and Pt^{2+} states. As can be seen from the spectra, the contributions from the platinum states depend on the sample microstructure. For example, the contributions from the observable states in the case of the sample containing clusters 0.3–0.5 nm in are as follows: state I, 34.0%; state II, 47.2%; state III,

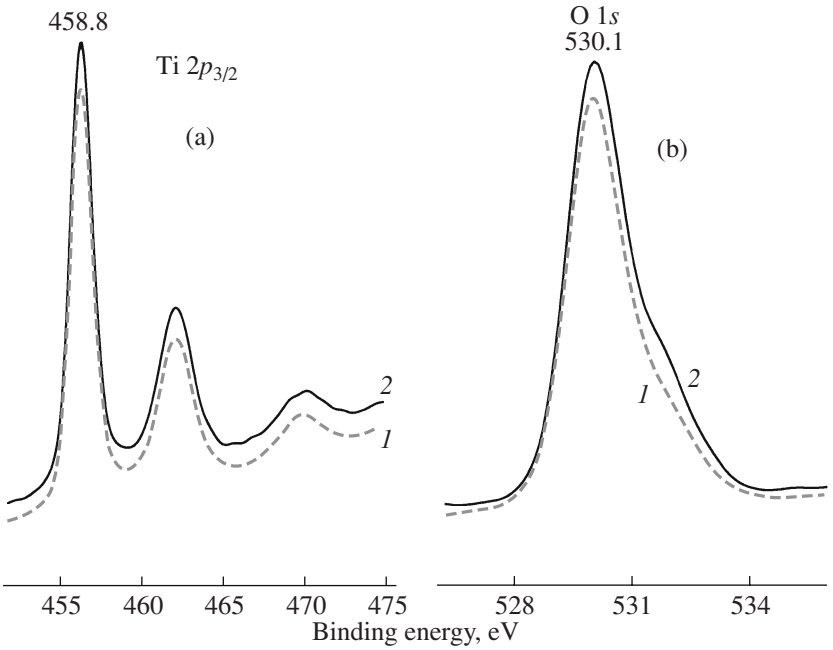

Fig. 8. (a) Ti $2p_{3/2}$ and (b) O 1*s* XPS spectra of $Pt/CeO_2–TiO_2$ catalysts with platinum particle sizes of (*1*) 0.3–0.5 and (*2*) 2–5 nm.

18.8%. For the sample containing platinum particles 2–5 nm in size, the contributions from these states are as follows: state I, 54.0%; state II, 26.6%; state III, 19.4%. Therefore, for the catalyst containing ultrafine platinum clusters 0.3–0.5 nm in size, the contribution from the ionic platinum state is essentially higher than for the catalyst containing platinum particles 2–5 nm in size.

The IR spectra of CO adsorbed on the catalysts are shown in Figs. 12 and 13. As can be seen from Fig. 12, the spectrum of the $Pt/CeO_2–TiO_2$ catalyst containing platinum clusters 0.3–0.5 nm in size contains three peaks due to CO adsorbed on platinum particles. The low-intensity absorption band at 1840 cm^{-1} is assigned to the bridging form of adsorbed CO [43]. This form practically does not interact with CO in the process of CO_2 formation [39, 46]. The second, most intense, symmetrical peak occurs at 2100 cm^{-1} and is assignable to the linear form of adsorbed CO [44, 45]. According to published data, this form is responsible for CO_2 formation [39, 46]. The position of this band points to rather weak bonding between the platinum particles and the CO molecules. It differs markedly from the positions of the same band for the Pt^0–CO complexes in Pt/TiO_2, Pt/CeO_2, and Pt/Al_2O_3 catalysts (2096–

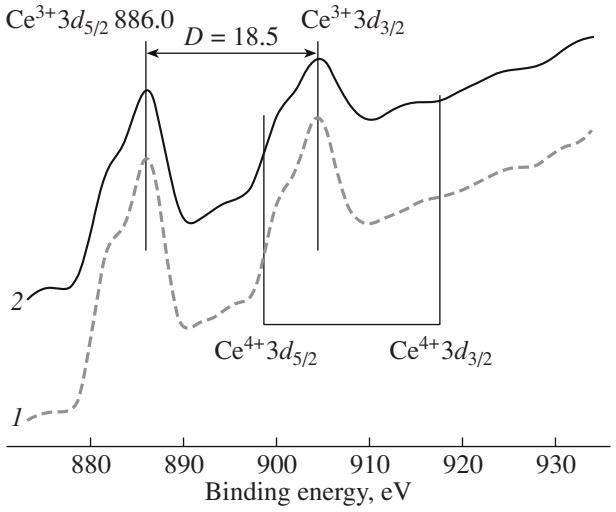

Fig. 9. Ce 3*d* XPS spectra of $Pt/CeO_2–TiO_2$ catalysts with platinum particle sizes of (*1*) 0.3–0.5 and (*2*) 2–5 nm.

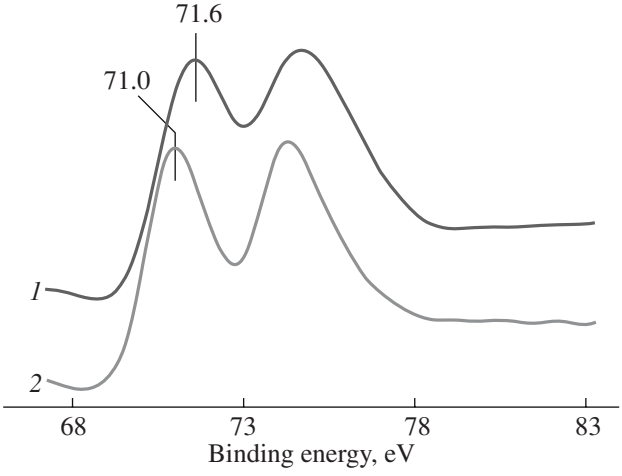

Fig. 10. Pt 4*f* XPS spectra of $Pt/CeO_2–TiO_2$ catalysts with platinum particle sizes of (*1*) 0.3–0.5 and (*2*) 2–5 nm.

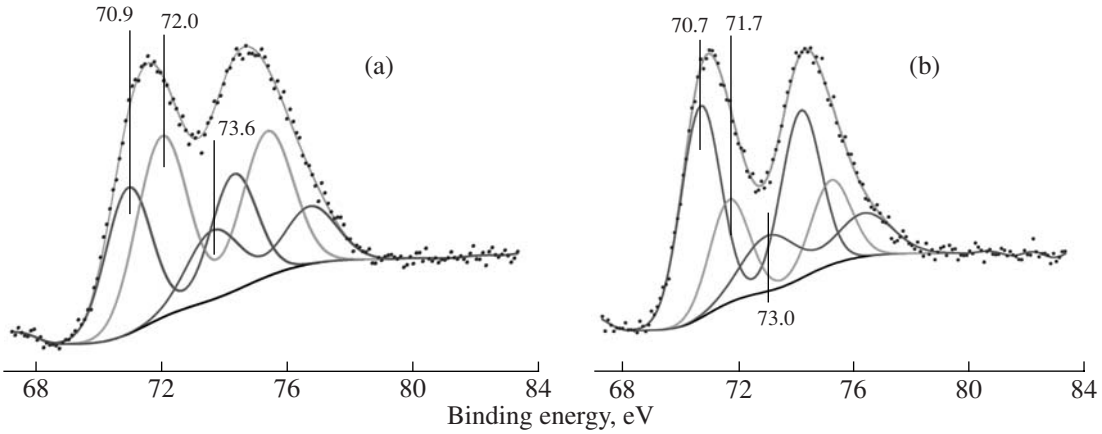

Fig. 11. Pt 4*f* spectra and their deconvolution into doublets taking into account the nonlinear Shirley-type background for Pt/CeO_2–TiO_2 catalysts with platinum particle sizes of (a) 0.3–0.5 and (b) 2–5 nm.

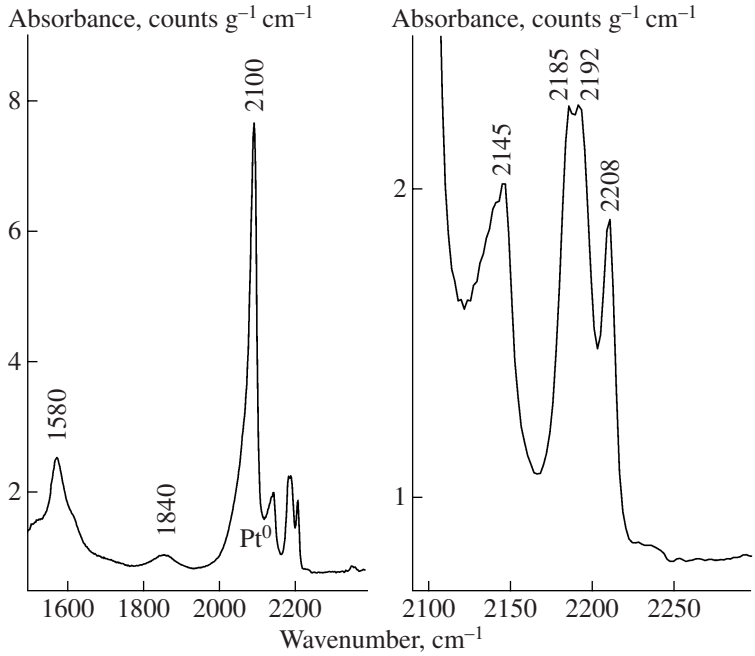

Fig. 12. IR spectrum of CO adsorbed on the Pt/CeO_2–TiO_2 catalyst with a platinum particle size of 0.3–0.5 nm.

2041 cm^{-1}) [39, 44, 45]. Based on data published in [44, 45], the absorption band at 2100 cm^{-1} can be assigned to the linear form of CO absorbed on platinum metal atoms having platinum ions as the nearest neighbors. This point, however, requires thorough examination. For the catalyst containing fine platinum, we observe a weak band at 2145 cm^{-1}, which, according to [39, 44, 45], is assignable to CO adsorbed on ionic platinum. Besides, this catalyst shows absorption bands at 2185–2220 cm^{-1}, which are characteristic of the Lewis acid sites of the support [43, 47]. As can be seen from the data obtained, CO adsorption on the Pt/CeO_2–TiO_2 catalyst containing ultrafine platinum clusters (0.3–0.5 nm) occurs mainly at Pt^0 atoms containing ionic platinum in the nearest neighborhood, not at ionic platinum. At the same time, as follows from XPS spectra, the ionic platinum content of the clusters is rather high. It is likely the Pt^0 state with $Pt^{\delta+}$ ions as the nearest neighbors is responsible for the weak Pt^0–CO binding, which ensures the high catalytic activity of the sample.

The IR spectrum of CO adsorbed on the Pt/CeO_2–TiO_2 catalyst with platinum particles 2–5 nm in size (Fig. 13) also exhibits adsorption bands at 2100 and 2145 cm^{-1}, but their intensities are essentially smaller than are observed for the previous catalyst. This is probably due to the increase of the platinum particle

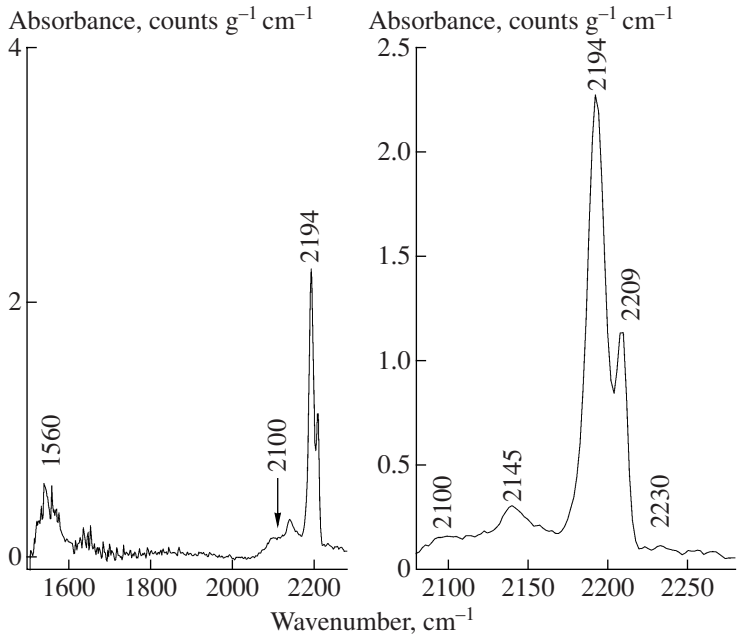

Fig. 13. IR spectrum of CO, adsorbed on the $Pt/CeO_2–TiO_2$ catalyst with a platinum particle size of 2–5 nm.

size. Also it is not improbable that the decrease of CO adsorption is caused by the partial coating of the active component by the support material due to the strong interaction between platinum and the support, even though the results of electron microscopy testify against this interaction. The absorption bands observed at 2185–2200 cm^{-1} are assigned to the acid sites of the support and are not discussed here. The growth of the platinum particles and the simultaneous change of their electronic state result in a decrease in the concentration of surface Pt^0 atoms forming loosely bonded complexes with CO molecules. This is the likely cause of the observed decrease of catalytic activity.

Thus, as follows from the above data, the modification of titanium dioxide with cerium oxide yields a $CeO_2–TiO_2$ support. This support has a nanocrystal structure consisting of irregularly intergrown anatase crystallites 3–6 nm in size. These crystallites form interblock boundaries, which is the place in which the Ce^{3+} ions are stabilized. Platinum is stabilized as clusters 0.3–0.5 nm in size mainly at these interblock boundaries, where the anatase structure is most heavily disordered. Apparently, the formation of the nanocrystal structure of the support in the presence of cerium is responsible for the stabilization of the ultrafine platinum clusters in the $Pt/CeO_2–TiO_2$ catalysts. This takes place via the formation of larger platinum particles 3–5 nm in size by the deposition of platinum on titanium dioxide with a regular anatase structure. XPS data show that, in fine clusters, platinum is in the metallic and ionic states. It should be noted that the platinum clusters 0.3–0.5 nm in size are rather stable to thermal treatment in an oxidative atmosphere. At the same time, under conditions of catalyst reduction with hydrogen, the microstructure changes already at 250°C, resulting in the aggregation of the ultrafine platinum clusters into larger particles 2–5 nm in size. The causes of the aggregation of the ultrafine platinum clusters during reduction are not known for certain, but it can be assumed that it is the increase of the platinum metal concentration in the clusters that favors their aggregation because the electronic state of titanium and cerium ions and the microstructure of the support remain unchanged. The change in the microstructure results in changes in the electronic state of platinum particles: XPS data indicate a marked increase of the platinum metal concentration in the particles 2–5 nm in size.

This investigation shows that the microstructure has a significant effect on the catalytic properties of the samples. The catalyst containing ultrafine platinum clusters 0.3–0.5 nm in size is much more active than the catalyst with clusters 2–5 nm in size. As follows from the above IR spectra, the high activity of the catalysts in CO oxidation might be a result of CO adsorption on platinum in linear form with the formation of weakly bonded Pt^0–CO complexes. According to published data, the presence of $Pt^{\delta+}$ in the nearest neighborhood of Pt^0 is responsible for this weak bonding. As follows from our data, the concentration of these complexes in the catalyst containing ultrafine platinum clusters is much higher than in the catalyst with platinum particles 2–5 nm in size. Apparently, the decrease of the concentration of weakly bonded Pt^0–CO complexes may have two causes. The first is the decrease in the extent of dispersion of platinum resulting in a decrease in the surface concentration of Pt^0 atoms. The second is the changes of their electron state. Our results agree with the data indicating that the maximum particle size of

supported metal at which one can expect changes in electronic properties is ~2 nm [14]. Therefore, the loss of the catalytic activity of Pt/CeO_2–TiO_2 in CO oxidation with a rise in the size of platinum particles can be explained by the decrease of the extent of dispersion of platinum and by changes in its electronic state.

ACKNOWLEDGMENTS

The authors thank A.S. Bobrin for catalytic measurements.

REFERENCES

1. Zhang, C.J. and Hu, P., *J. Am. Chem. Soc.*, 2001, vol. 123, p. 1166.
2. Rumpf, F., Poppa, H., and Boudart, M., *Langmuir*, 1988, vol. 4, p. 722.
3. Falconer, J.L. and Magrini-Bair, K.A., *J. Catal.*, 1998, vol. 179, p. 171.
4. Blake, N.R. and Griffin, G.L., *J. Phys. Chem.*, 1988, vol. 92, p. 5697.
5. Obee, T.N. and Hay, S.O., *Environ. Sci. Technol.*, 1997, vol. 31, p. 2034.
6. Anderson, M.A., Yamazaki-Nishida, S., and Cervera-March, S., in *Photocatalytic Purification and Treatment of Water and Air*, Ollis, D.F. and Al-Ekabi, H., Eds., Amsterdam: Elsevier, 1993, p. 405.
7. Fu, X.F., Zelter, W.A., and Anderson, M.A., *Appl. Catal., B*, 1995, vol. 6, p. 209.
8. Dulub, O., Hebenstreit, W., and Diebold, U., *Phys. Rev. Lett.*, 2000, vol. 84, no. 16, p. 3646.
9. Anderson, J.R., *Structure of Metallic Catalysts*, London: Academic, 1975.
10. Harris, P.J.F., *Int. Mater. Rev.*, 1995, vol. 40, p. 97.
11. Bukhtiyarov, V.I. and Slin'ko, M.G., *Usp. Khim.*, 2001, vol. 70, no. 2, p. 167.
12. Abbet, S., Heiz, U., Häkkimen, H., and Landman, U., *Phys. Rev. Lett.*, 2001, vol. 86, p. 5950.
13. Heiz, U., Sanches, A., Abbet, S., and Schneider, W.-D., *J. Am. Chem. Soc*, 1999, vol. 121, p. 3214.
14. Kubo, R., *J. Phys. Soc. Jpn.*, 1962, vol. 17, p. 975.
15. Kobozev, N.I., *Zh. Fiz. Khim.*, 1939, vol. 13, p. 1.
16. Poltorak, O.M. and Boronin, V.S., *Zh. Fiz. Khim.*, 1966, vol. 40, p. 2671.
17. Van Hardeveld. R. and Hartog, F., *Adv. Catal.*, 1972, vol. 22, p. 75.
18. Bond, G.C., *Proc. 4th Int. Congr. on Catalysis*, Moscow, 1968, vol. 2, p. 266.
19. Hamilton, J.F. and Logel, P.C., *J. Catal*, 1973, vol. 29, p. 253.
20. Hamilton, J.F. and Baetzold, R.C., *Science*, 1979, vol. 205, p. 1213.
21. Bond, G.C., *Surf. Sci.*, 1985, vol. 156, p. 966.
22. Boudart, M., AIdag, A., Benson, J.E., Dougharty, N.A., and Girvin, C., *J. Catal.*, 1966, vol. 6, p. 92.
23. Boudart, M., *Adv. Catal.*, 1969, vol. 20, p. 153.
24. Goodman, D.W., Peden, C.H.F., Fisher, G.B., and Oh, S.H., *Catal. Lett.*, 1993, vol. 22, p. 271.
25. Bowker, M., Guo, Q., Li, Y., and Joner, R.W., *Catal. Lett.*, 1993, vol. 22, p. 275.
26. Gracia, F.J., Bollmann, L., Wolf, E.E., Miller, J.T., and Kropf, A.J., *J. Catal.*, 1966, vol. 220, p. 382.
27. Atalik, B. and Uner, D., *J. Catal.*, 1966, vol. 241, p. 268.
28. Thompson, M. and Walsh, J.N., *A Handbook of Inductively Coupled Plasma Spectrometry*, Glasgow: Blackie, 1983.
29. Guinier, A., *Theorie et technique de la radiocristallographie*, Paris: Dunod, 1956.
30. Barret, E.P., Joyner, L.G., and Hallenda, P.H., *J. Am. Chem. Soc*, 1951, vol. 73, no. 1, p. 373.
31. *Handbook of X-ray Photoelectron Spectroscopy*, Moulder, J.F., Stickle, W.F., Sobol, P.E., et al., Eds., Eden Prairie, Minn.: Perkin-Elmer, 1992.
32. *Handbook of X-ray Photoelectron Spectroscopy*, Wagner, C.D., Riggs, W.M., Davis, L.E., et al., Eds., Eden Prairie, Minn.: Perkin-Elmer, 1979.
33. Sherwood, R.M.A., *Practical Surface Analysis by Auger and X-ray Photoelectron Spectroscopy*, Briggs, D. and Seah, M.P., Chichester: Wiley, 1983.
34. Zenkovets, G.A., Tsybulya, S.V., Burgina, E.B., and Kryukova, G.N., *Kinet. Katal.*, 1999, vol. 40, no. 4, p. 623 [*Kinet. Catal.* (Engl. Transl.), vol. 40, no. 4, p. 562].
35. Bokii, G.B., *Kristallokhimiya* (Crystal Chemistry), Moscow: Mosk. Gos. Univ., 1960.
36. Leonov, A.I., Piryutko, M.M., and Keler, E.K., *Izv. Akad. Nauk SSSR, Ser. Khim.*, 1966, no. 5, p. 787.
37. Bazuev, G.V., Makarova, Shch.V., Zhilyaev, V.A., and Shveikin, G.P., *Zh. Neorg. Khim.*, 1976, vol. 21, no. 10, p. 1967.
38. Kuskov, V.D., Zverlin, A.V., Zaslavskii, A.M., Mel'nikov, A.V., and Slivinskaya, A.V., *Zh. Neorg. Khim.*, 1991, vol. 36, p. 2757.
39. Pozdnyakova, O., Teschner, D., Wootsch, A., Kröhnert, J., Steinhauer, B., Sauer, H., Toth, L., Jentoft, F.C., Knoh-Gericke, A., Paal, Z., and Schlögl, R., *J. Catal.*, 2006, vol. 237, p. 1.
40. Kryukova, G.N., Zenkovets, G.A., Shutilov, A.A., Wilde, M., Günter, K., Fassler, D., and Richter, K., *Appl. Catal., B*, 2007, vol. 71, p. 169.
41. Holgado, J.P., Alvazer, R., and Munuera, G., *Appl. Surf. Sci.*, 2000, vol. 161, p. 301.
42. Mullins, D.R., Overbury, S.H., and Yuntley, D.R., *Surf. Sci.*, 1998, vol. 409, p. 307.
43. Hadjiivanov, K.I. and Vayssilov, G.N., *Adv. Catal.*, 2002, vol. 47, p. 307.
44. Daniel, D.W., *J. Phys. Chem*, 1988, vol. 92, p. 3891.
45. Jin, T., Zhou, Y., Mains, G.J., and White, J.M., *J. Phys. Chem.*, 1987, vol. 91, p. 59 311.
46. Lokhov, Yu.A. and Davydov, A.A., *Kinet. Katal.*, 1980, vol. 21, no. 6, p. 1523.
47. Paukshtis, E.A., *Infrakrasnaya spektroskopiya v geterogennom kislotno-osnovnom katalize* (Infrared Spectroscopy in Heterogeneous Acid–Base Catalysis), Novosibirsk: Nauka, 1992.